

Elastic–plastic behavior of nickel-based single crystal superalloys with γ–γ' phases based on molecular dynamics simulations

Jing-Zhao Cao(曹景昭), Yun-Guang Zhang(张云光), Zhong-Kui Zhang(张中奎), Jiang-Peng Fan(范江鹏), Qi Dong(董琪), and Ying-Ying Fang(方盈盈)

Citation : Chin. Phys. B, 2025, 34 (**4**): 046204. DOI: 10.1088/1674-1056/adb40f
Journal homepage: http://cpb.iphy.ac.cn; http://iopscience.iop.org/cpb

What follows is a list of articles you may be interested in

A molecular dynamics study on mechanical performance and deformation mechanisms in nanotwinned NiCo-based alloys with nano-precipitates under high temperatures

Zihao Yu(于子皓), Hongyu Wang(王鸿宇), Ligang Sun(孙李刚), Zhihui Li(李志辉), and Linli Zhu(朱林利)
Chin. Phys. B, 2024, 33 (**11**): 116201. DOI: 10.1088/1674-1056/ad6cca

Temperature effect on nanotwinned Ni under nanoindentation using molecular dynamic simulation

Xi He(何茜), Ziyi Xu(徐子翼), and Yushan Ni(倪玉山)
Chin. Phys. B, 2024, 33 (**1**): 016201. DOI: 10.1088/1674-1056/acf997

Synthesis of flower-like WS_2 by chemical vapor deposition

Jin-Zi Ding(丁金姿), Wei Ren(任卫), Ai-Ling Feng(冯爱玲), Yao Wang(王垚), Hao-Sen Qiao(乔浩森), Yu-Xin Jia(贾煜欣), Shuang-Xiong Ma(马双雄), and Bo-Yu Zhang(张博宇)
Chin. Phys. B, 2021, 30 (**12**): 126201. DOI: 10.1088/1674-1056/ac0524

Plastic deformation mechanism transition of Ti/Ni nanolaminate with pre-existing crack: Molecular dynamics study

Meng-Jia Su(宿梦嘉), Qiong Deng(邓琼)†, Min-Rong An(安敏荣), and Lan-Ting Liu(刘兰亭)
Chin. Phys. B, 2020, 29 (**11**): 116201. DOI: 10.1088/1674-1056/aba2e5

Effects of helium implantation on mechanical properties of $(Al_{0.31}Cr_{0.20}Fe_{0.14}Ni_{0.35})O$ high entropy oxide films

Zhao-Ming Yang(杨朝明), Kun Zhang(张坤), Nan Qiu(裘南), Hai-Bin Zhang(张海斌), Yuan Wang(汪渊), Jian Chen(陈坚)
Chin. Phys. B, 2019, 28 (**4**): 046201. DOI: 10.1088/1674-1056/28/4/046201

Elastic–plastic behavior of nickel-based single crystal superalloys with γ–γ' phases based on molecular dynamics simulations

Jing-Zhao Cao(曹景昭), Yun-Guang Zhang(张云光), Zhong-Kui Zhang(张中奎)†, Jiang-Peng Fan(范江鹏), Qi Dong(董琪), and Ying-Ying Fang(方盈盈)

School of Science, Xi'an University of Posts and Telecommunications, Xi'an 710121, *China*

(Received 27 November 2024; revised manuscript received 12 January 2025; accepted manuscript online 8 February 2025)

The effects of temperature and Re content on the mechanical properties, dislocation morphology, and deformation mechanism of γ–γ' phases nickel-based single crystal superalloys are investigated by using the molecular dynamics method through the model of γ–γ' phases containing hole defect. The addition of Re makes the dislocation distribution tend towards the γ phase. The higher the Re content, the earlier the γ phase yields, while the γ' phase yields later. Dislocation bends under the combined action of the applied force and the resistance of the Re atoms to form a bend point. The Re atoms are located at the bend points and strengthen the alloy by fixing the dislocation and preventing it from cutting the γ' phase. Dislocations nucleate first in the γ phase, causing the γ phase to deform plastically before the γ' phase. As the strain increases, the dislocation length first remains unchanged, then increases rapidly, and finally fluctuates and changes. The dislocation lengths in the γ phase are larger than those in the γ' phase at different temperatures. The dislocation length shows a decreasing tendency with the increase of the temperature. Temperature can affect movement of the dislocation, and superalloys have different plastic deformation mechanisms at low, medium and high temperatures.

Keywords: nickel-based single crystal superalloys, elastic–plastic behavior, dislocations, molecular dynamics simulation

PACS: 62.25.–g, 62.20.F–, 61.72.Lk, 02.70.Ns

DOI: 10.1088/1674-1056/adb40f **CSTR:** 32038.14.CPB.adb40f

1. Introduction

Nickel-based single crystal superalloys are widely used in the hot-end components of aero-engines and gas turbines due to their excellent high-temperature mechanical properties and high temperature corrosion resistance.[1–4] The increasingly demanding design and performance requirements of advanced aero-engines have also put forward higher requirements for the development of these superalloys. Nickel-based single crystal superalloys have a typical γ and γ' two-phase structure, and the size and percentage of the γ and γ' phases, as well as the type and distribution of elements in the two-phase, have a direct impact on the properties of the alloy.[5–7] While the two-phase structure enhances the high temperature mechanical properties of single crystal superalloys, cracks, and holes are also prone to form at the two-phase interface. This becomes one of the important causes of superalloys failure. The lattice mismatch makes the two-phase interface an important source of dislocations, and its effect on plastic deformation is currently less well understood.

The tensile deformation mechanism of single crystal superalloys has significant temperature dependence. Tensile test studies.[8–12] have found that the plastic deformation of superalloys at room temperatures is mainly manifested by dislocations and stacking faults shearing into the γ' phase. Some scholars believe that there is also antiphase boundary shearing into the γ' phase. The plastic deformation of superalloys at medium temperatures is mainly manifested by the shear of stacking faults and antiphase boundaries into the γ' phase. The plastic deformation of superalloys at high temperatures is primarily characterized by Orowan bypassing and dislocation climbing, alongside antiphase boundary shearing into the γ' phase. The most typical microscopic features of the deformation of nickel-based single crystal superalloys are manifested as the movement of dislocations and rafting of γ' phase. The experimental study can visually observe the microstructural evolution and dislocation morphology of the material. This also provides direct evidence for studying the plastic deformation mechanism of materials. However, we are unable to observe intuitively the motion and change laws of atoms in the material deformation process, which also hinders further exploration of the material deformation mechanism in the microphysical mechanism. Molecular dynamics simulations can effectively study material deformation (atomic motion, dislocation nucleation, dislocation motion, etc.) at the atomic scale. They have been widely used in recent years to characterize the mechanical properties and microscopic deformation mechanisms of nickel-based single crystal superalloys. The main findings include:[13–16] (i) For single crystal superalloys without rhenium (Re), the higher the temperature, the earlier the dislocations form, and the lower Young's modulus and yield stress of the superalloy. (ii) The smaller the relative radius of the hole defect at the γ–γ' two-phase interface, the

†Corresponding author. E-mail: zkzhang@xupt.edu.cn

© 2025 Chinese Physical Society and IOP Publishing Ltd. All rights, including for text and data mining, AI training, and similar technologies, are reserved.

higher the yield stress of the superalloy. (iii) Stair-rod dislocations and Shockley dislocations are the main forms of γ phase plastic deformation. Dislocations slip and expand along the $\{111\}$ planes, and as the temperature increases, more $\{111\}$ slip planes are activated. (iv) Under fatigue loading, the main deformation mechanism of single crystal superalloys in the temperature range of 300 K–800 K is dislocations and stacking faults shearing into γ' phase. In the temperature range of 1000 K–1500 K, it is mainly Orowan bypassing and climbing, accompanied by a small amount of cross-slip. In the temperature range of 800 K–1000 K, the deformation mechanism transitions from dislocations and stacking faults shearing into γ' phase to Orowan bypassing and climbing. However, there is still a lack of a clear and unified understanding of the deformation mechanism of nickel-based single crystal superalloys at different temperatures. The experimental and simulation results are relatively dispersed. Considering the influence of the Re element makes the problem more complicated.

In the development of nickel-based single crystal superalloys, the core element Re plays the greatest role in improving their high temperature mechanical properties. The content of Re has become one of the most important differences between different generations of these superalloys.[17–19] In complex environments such as high temperatures and cyclic loading, Re has a significant effect on the nucleation and movement of dislocations and the rafting of the γ' phase.[13,20] Re can strengthen the γ phase and inhibit the growth of the γ' phase.[18,21] It also reduces the interfacial energy of the two-phase and retards the coarsening of the γ' phase,[2,22–24] and improves the lattice mismatch of the superalloys.[20] Re atoms can diffuse with the movement of dislocations, and the Re atoms enriched at the dislocations can hinder the movement of dislocations, reduce the creep rate, and enhance the creep properties of the alloy.[13,15] The addition of Re reduces the stacking fault energy, promotes the formation of stacking faults, and improves the stability of the alloy microstructure, resulting in better fatigue properties.[13,24,25] However, the addition of Re not only improves the mechanical properties of the superalloys but also promotes the precipitation of a brittle topologically close-packed (TCP) phase at high temperatures.[20] The TCP phase is prone to initiating cracks and holes, making it a significant cause of material fracture failure.[20,26,27] At the same time, The Re element is a strategically scarce resource, adding 1% content of Re will double the casting cost of single crystal superalloys. This requires essentially studying the strengthening mechanism of the Re element and its influence on superalloys deformation, and therefore looking for potential alternative elements to reduce the production cost of alloys and promote the development of higher performance single crystal superalloys. Molecular dynamics methods can help clarify this issue on the atomic scale.

In this paper, based on the molecular dynamics methods, a two-phase model of γ–γ' containing hole defect is established to study the mechanical properties, dislocation morphology, and deformation mechanism of the γ–γ' two-phase of nickel-based single crystal superalloys at different temperatures and Re contents under tensile stress.

2. Simulation models and methods

The two-phase structure of the nickel-based single crystal superalloys was simulated to model the γ phase composed of Ni atoms and the γ' phase composed of Ni_3Al. In the model, 0%, 1%, 2%, 3%, 4%, and 5% of the Re atoms were added, respectively. According to the determination results of the Re element content in the γ–γ' two-phase material by the atom probe tomography[24] and the energy-dispersive x-ray spectroscopy,[28] 95% of Re atoms randomly replaced Ni atoms in the γ phase, and the remaining 5% randomly replaced Ni atoms in the γ' phase. There was a hole defect at the interface of the two phases, with a pore diameter of 35.465 Å, as shown in Fig. 1. The lattice parameters of the γ–γ' phases in the model are $a_\gamma = 3.52$ Å and $a_{\gamma'} = 3.573$ Å. In order to minimize the lattice mismatches, the γ phase has the dimensions of $67a_\gamma \times 20a_\gamma \times 67a_\gamma$ and the γ' phase has the dimensions of $66a_{\gamma'} \times 20a_{\gamma'} \times 66a_{\gamma'}$, and there are a total of 701380 atoms in the model, with X–Y–Z axes in the [100]–[010]–[001] directions. Periodic boundary conditions were imposed on the model and the system was brought to equilibrium by relaxing 50000 steps under an isothermal and isobaric system. The model was subjected to uniaxial stretching along the X-axis at a strain rate of 1×10^9 s^{-1}, and the stretching was stopped when the strain reached 20%, at temperatures of 300 K (low temperature), 1033 K (medium temperature), and 1253 K (high temperature). The large-scale atomic/molecular massively parallel simulator (LAMMPS)[29] was used to perform molecular dynamics simulations. The Ni–Al–Re embedded atom potential developed by Du *et al.*[30] and the Ni–Al embedded atom potential developed by Pun *et al.*[31] were used, and the above potential functions can describe the interactions between Ni–Al–Re and Ni–Al better. The visualization was carried out by Ovito[32] and the dislocation analysis[33] method was applied to study the microscopic mechanism of the structural changes of the two-phase during stretching.

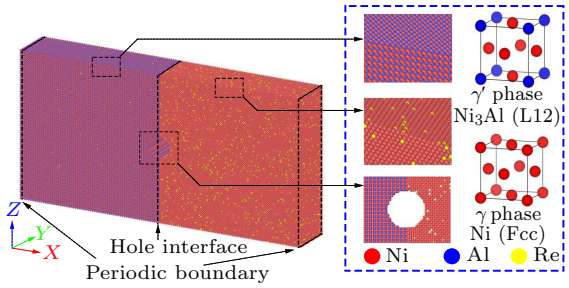


Fig. 1. Molecular dynamics model.

3. Results and discussion

3.1. Effect of Re content on plastic deformation and dislocation

Figure 2(a) shows the stress–strain curves of the model at different Re contents. As the Re content increases, the yield stress and yield strain of the material gradually decrease, making the material more prone to yielding and undergoing plastic deformation. After reaching the yield point, the stress decreases rapidly, and then with the increase of strain, the stress changes steadily within a certain range, and the deformation of the material is relatively stable. Further observation of the dislocation distribution within the two-phase when the stress begins to stabilize in Fig. 2(b) reveals. At 0% Re content, the dislocation is mainly distributed in the γ' phase. When Re is added, the dislocation distribution tends to the γ phase. In the range of 0%–2% Re contents, the proportion of dislocations in the γ' phase decreases with the increase of Re content. In the range of 2%–5% Re contents, the proportion of dislocations in the γ' phase increases with the increase of Re content. Figures 2(c1)–2(h1) show the microstructure at the yield of the γ phase at different Re contents, corresponding to 0%, 1%, 2%, 3%, 4% and 5% Re, respectively. As the Re content increases, the γ phase yields more easily. The γ phase has the largest yielding strain at 0% Re content and the smallest at 5% Re content. When yielding occurs, dislocations nucleate first in the

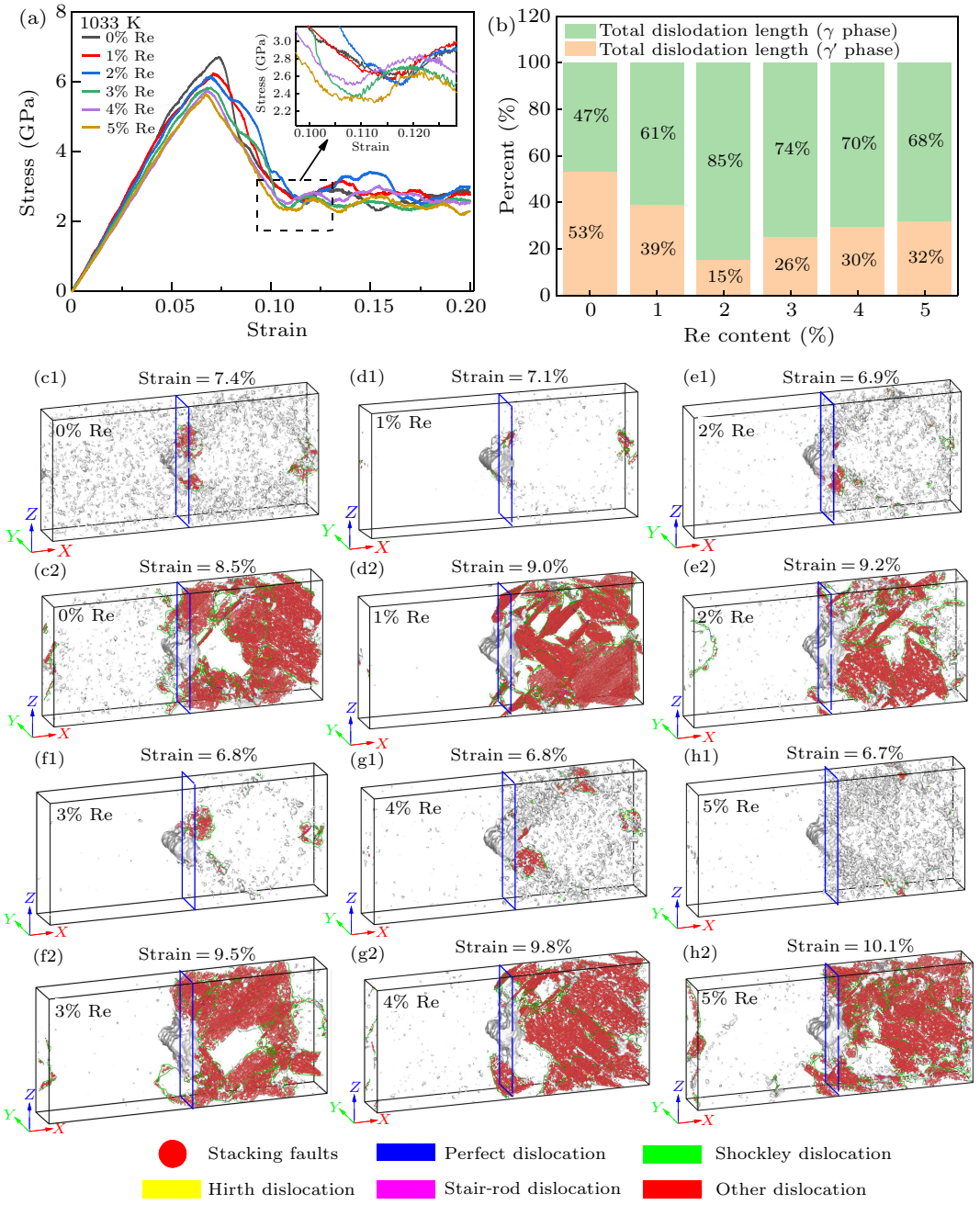


Fig. 2. Stress–strain curves, the proportion of dislocations in the two-phase, and microstructures of γ and γ' phases at yield for materials with different Re contents: (a) stress–strain curves, (b) the proportion of dislocations in the two-phase when the stress begins to stabilize, (c1)–(h1) the microstructure of the γ phase at yield under different Re contents, (c2)–(h2) the microstructure of the γ' phase at yield under different Re contents.

γ phase, indicating that plastic deformation begins in the γ phase. As strain increases, dislocations in the γ phase start to cut through the two-phase interface into the γ' phase, causing it to undergo plastic deformation, as shown in Figs. 2(c2)–2(h2). The yielding strain of the γ' phase increases with increasing Re content. The γ' phase has the smallest yielding strain at 0% Re content and the largest at 5% Re content. The Re content affects the plastic deformation of the γ–γ' phases in nickel-based single-crystal alloys. With increasing Re content, the γ phase yields earlier, while the yielding of the γ' phase becomes later.

Compared to atoms like Ni and Al in the superalloys, Re atoms have a lower diffusion rate. When dislocations move to Re atoms, they are hindered by Re atoms, as shown in Fig. 3. In superalloys with different Re contents, Re atoms can be observed on dislocation lines within both the γ and γ' phases. The moving dislocations are hindered by Re atoms, causing them to bend. In the red box of the microscopic magnification, the bending phenomenon of the dislocation, with Re atoms as the bending points, can be seen. This indicates that Re atoms strongly hinder the movement of the dislocation. Under the combined effects of external forces and the resistance offered by Re atoms, the dislocation bends at the locations of Re atoms, forming kinks. This phenomenon is commonly referred to as the "pinning" effect of Re atoms on dislocation.[22]

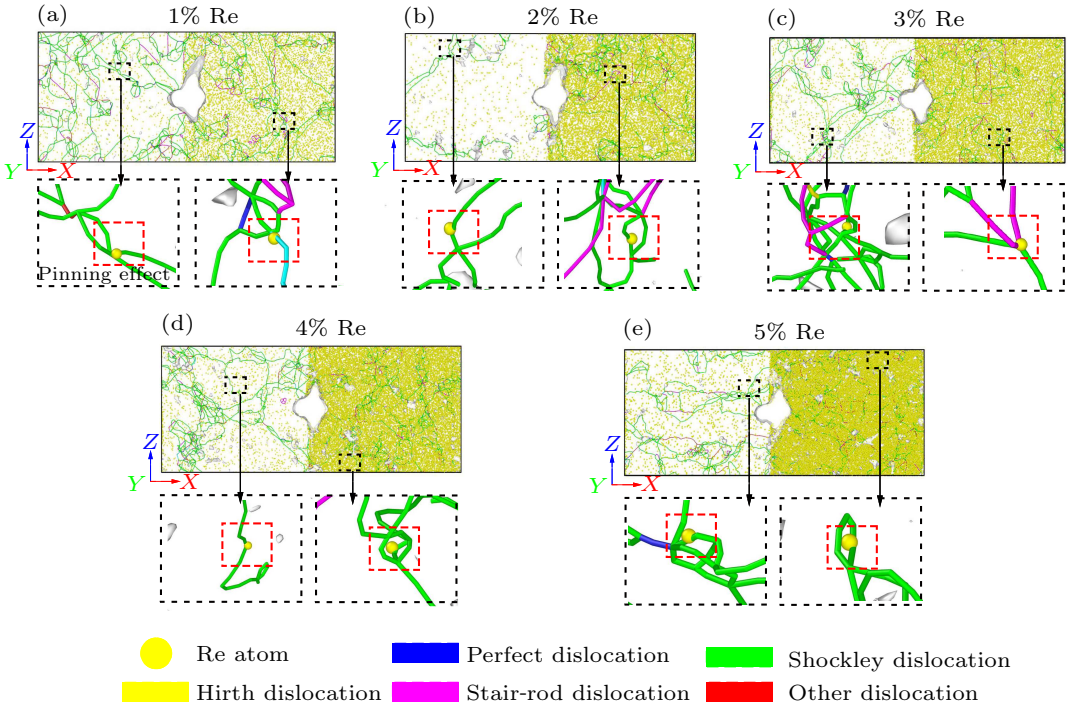


Fig. 3. The pinning effect of Re atoms on dislocations: (a) 1% Re, (b) 2% Re, (c) 3% Re, (d) 4% Re, (e) 5% Re.

In conclusion, the Re element content has a significant effect on the plastic deformation and dislocation of the γ–γ' phase of nickel-based single crystal superalloys. With the increase of Re content, the stacking fault energy of the γ phase decreases.[13,23] The γ phase is more likely to generate dislocations and stacking faults and is more prone to plastic deformation. The addition of Re not only hinders the movement of the dislocation to the two-phase interface but also strengthens the two-phase interface.[34] They retard the cut of the dislocations into the γ' phase, resulting in a higher yield strain in the γ' phase of superalloys with higher Re content. At 0% Re content, there is a lack of Re atomic pinning effect and interface strengthening effect. A large number of dislocations cut into the γ' phase, and the proportion of dislocations in the γ' phase is the largest. A large number of dislocations proliferate and expand in both γ and γ' phases. Therefore, at 0% Re, the material has the most dislocations. With the increase of strain, once the dislocation cuts through the two-phase interface into the γ' phase, the strengthening effect of the two-phase interface will be weakened. In the range of 0%–2% Re contents, with the increase of Re content, the dislocation of cutting into the γ' phase gradually decreases, and the proportion of dislocations in the γ' phase decreases. Compared to superalloys without Re, there is a small amount of dislocation proliferation and expansion in the γ' phase, which causes the dislocation length of the material to decrease as the Re content increases. In the range of 0%–2% Re contents, the inhibition effect of Re on dislocation is gradually enhanced. In the range of 2%–5% Re contents, lower stacking fault energy can promote the generation and decomposition of dislocation.[15] When the γ' phase has plastic deformation, compared with the low Re superalloys, with the increase of strain, the number of dislocations cut into the γ' phase gradually increases. More dislocations proliferate and expand in the γ' phase, and the dislocation length

of the material increases with the increase of Re content. The inhibition effect of the increase of Re content on the cutting and proliferation of the dislocation is weakened. This suggests that a 2%-Re content is a critical point. If the content is lower than this, the inhibitory effect of Re on dislocation is enhanced. Above this content, the inhibitory effect of Re on dislocation is weakened. In addition, when the Re content is 2%, the alloy has a higher yield stress, and the stress drop is the slowest. When the deformation is stable, the dislocations cut into the γ' phase are the least, and the γ' phase has the best strengthening effect relative to superalloys. Therefore, 2%-Re content is chosen as the best doping concentration for further study.

3.2. Tensile mechanical properties of γ–γ' phase at different temperatures

The tensile stress–strain curves, Young's modulus, and yield stress of the nickel-based single crystal superalloys γ–γ' two-phase model at different temperatures are shown in Fig. 4. From Fig. 4(a), it can be seen that at 300 K and 1033 K, the stress increases and then decreases with the increase of strain and then gradually stabilizes. At 1253 K, the stress increases and then decreases as the strain increases, and the model fractures at a strain of 12.3%. It can be seen that temperature has a significant effect on the deformation and fracture of the two-phase. The higher the temperature, the more prone the model is to deformation and fracture. In the elastic deformation stage, stress increases linearly with strain. At 300 K, 1033 K, and 1253 K, Young's modulus is 121.31 GPa, 88.84 GPa, and 78.15 GPa, respectively, as shown in Fig. 4(b). The results show that the higher the temperature, the smaller the Young's modulus and the weaker the ability of the model to resist the elastic deformation. Yielding occurs when strain reaches a critical value. From Fig. 4(c), the yield stress and strain at 300 K are 9.22 GPa and 7.6%, respectively. At 1033 K, they are 6.13 GPa and 6.9%. And at 1253 K, they are 5.08 GPa and 6.5%. The yield strains at different temperatures are relatively close, and the yield strain decreases slightly with the increase in temperature. This indicates that temperature has a minor effect on yield strain, and the model has relatively stable yield strains at different temperatures. However, as the temperature increases, the yield stress decreases significantly, and the plastic deformation resistance decreases significantly. The yield stress and yield strain show the same pattern of change with increasing temperature at 0%, 5%, and 9% Re contents.[15] At low and medium temperatures, the stress–strain curves begin to fluctuate at 10.1% and 10.4% of strains, respectively, and the model enters the stable deformation stage. At high temperatures, the slope of the stress–strain curve changes significantly at 10.4% of strain. The deformation of the model intensified and entered the stage of rapid fracture. In Fig. 4(a), the stress–strain curves approximately intersect at 10.5% strain, when approximately the same stress is required for the same strain, and the stress–strain relationship changes significantly at different temperatures near this point. In other molecular dynamics simulations, a similar strain threshold of 10.5% has been found.[15] Beyond this strain point, the change in the stress–strain relationship is affected by temperature.

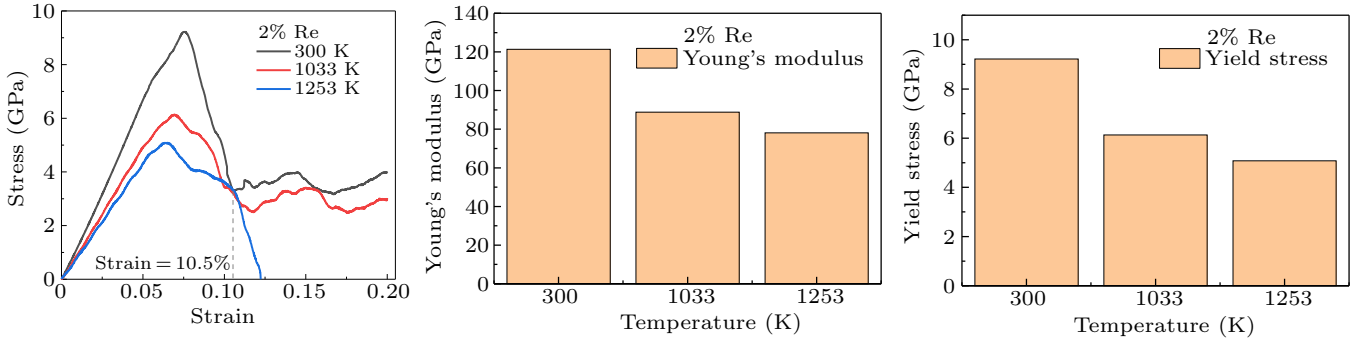


Fig. 4. Tensile mechanical properties of γ–γ' phase at different temperatures (2% Re): (a) stress–strain curve, (b) Young's modulus, (c) yield stress.

At medium and low temperatures, the ability of the two-phase to resist deformation changes with the accumulation of strains. It shows that it has a stable ability to resist deformation in the elastic stage, and the deformation resistance decreases rapidly after yielding. In the later stage of deformation, the deformation resistance tends to be stable, showing a small range of fluctuation characteristics. At high temperature, the model has stable deformation resistance in the elastic stage, and the plastic deformation resistance decreases rapidly and fractures after yielding.

The macroscopic properties of the material are a direct manifestation of its microstructural characteristics. Figure 5 shows the stress–strain curves of the model at 1033 K and the microscopic morphology of the γ–γ' two-phase at the corresponding node. From Fig. 5, it can be seen that from the beginning of loading to the elastic deformation of the model at point A, the stress–strain relationship remains linear, and the OA section is the first deformation stage. At a strain of 6.9% (point A), the stress reaches a maximum, a small number of dislocations and stacking faults are generated in the γ phase, and the yielding of the γ phase occurs. When the strain increases to 9.2% (point B), a small amount of Shockley dislo-

cations cut the hole interface and periodic boundary into the γ' phase, and the γ' phase begins to yield. The dislocations are mainly distributed in the γ phase, and the AB section is the second stage of the deformation. As the strain increases to 20% (point C), more dislocations cut the two-phase interface into the γ' phase, and the dislocation density difference in the two phases decreases. The stress–strain curve in the late stage of deformation shows a zigzag flow characteristic, and the BC section is the third stage of deformation.

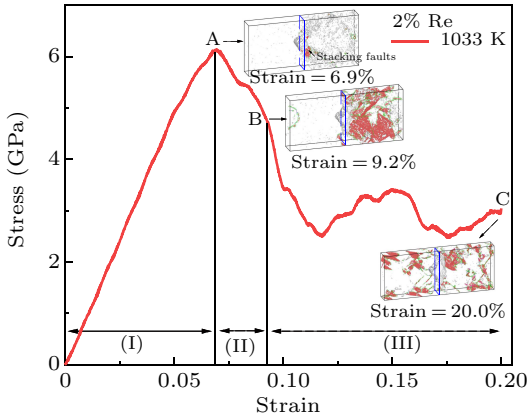


Fig. 5. Microscopic morphology of γ–γ' two-phase at different stress strains (2% Re).

The potential energy of the Ni model is higher than that of the Ni_3Al model. Under the same energy conditions, Ni–Ni atomic bonds are more easily broken,[35] making dislocations nucleate first in the γ phase. This causes the γ phase to deform plastically before the γ' phase. The asynchronism plastic deformation of the two phases leads to greater stress concentration at their interface. As the strain increases, the dislocations proliferate and move rapidly in the γ phase. The plastic deformation resistance of the model is weakened, so the stress gradually decreases with the increase of strain after point A. At the two-phase interface, the Ni–Al bonds in the γ' phase are unstable due to higher stress concentration. Dislocations in the γ phase cut through the interface into the γ' phase. This weakens the plastic deformation resistance of the model, causing the stress to decrease further with increasing strain after point B. As strain increases, more dislocations cut through the two-phase interface into the γ' phase. Dislocations continue to proliferate, move, interact, and annihilate, eventually reaching a dynamic equilibrium. The plastic deformation of the two phases is gradually approaching. The stress–strain curve in the later stage of deformation shows a jagged flow characteristic.

3.3. Dislocation lengths at different temperatures

The proliferation and movement of dislocations are microscopic manifestations of material plastic deformation. During the model deformation process, as shown in Fig. 6(a). With the increase of strain, the length of the dislocation is unchanged at first, then increases rapidly, and finally fluctuates and changes. The elastic deformation stage, where the dislocation length is approximately zero and remains essentially constant with increasing strain, corresponds to the stage of rapid stress growth in Fig. 4. After yielding, the model begins to deform plastically. Dislocations continue to proliferate and move within the model, causing their length to increase rapidly. The model exhibits "softening" characteristics, corresponding to the stage of rapidly decreasing stress in Fig. 4. According to Fig. 6, when the strain is 10.5%, the dislocation length changes with the strain, which corresponds to the change of the stress–strain curve at 10.5% strain in Fig. 4. At the late stage of deformation, the plastic deformation gradually stabilizes and the length of dislocation at the same strain decreases with the increase of temperature. According to dislocation theory, the strain rate of the material is proportional to the density of the movable dislocation, the velocity of the dislocation, and the Burgers vector of the dislocation.[15] When the model deforms at a constant rate, temperature increases, dislocation motion speeds up, and internal dislocation density decreases, resulting in shorter dislocation lengths at high temperatures.

Overall, the dislocations are mainly distributed in the γ phase at different temperatures, as shown in Fig. 6(b). The dislocations are mainly nucleated in the γ phase, and the γ phase undergoes the main plastic deformation. As the temperature increases, the motion of atoms intensifies, and dislocations are more likely to nucleate and have a greater rate of motion. According to Fig. 6(b), the higher the temperature, the larger the length of dislocations in the γ phase at the same strain in the initial stage of plastic deformation. As the strain continues to increase, dislocations in the γ phase cut through the two-phase interface into the γ' phase or interact and annihilate during movement.[13] At the same strain in the middle and late stages of deformation, the γ phase has a larger dislocation length at medium temperature, indicating the greatest difference in dislocation lengths between nucleation and annihilation within the γ phase at this time. At low temperature, dislocations are not easy to nucleate and move, while at high temperature, they nucleate and move more easily. Dislocation lengths are longer at high temperature than at low temperature, suggesting that dislocation nucleation primarily affects the length of dislocations in the γ phase. At high temperature, dislocations in the γ' phase are more likely to move to the hole interface and annihilate. Therefore, the higher the temperature, the smaller the dislocation length in the γ' phase, as shown in Fig. 6(b). It can be seen that the motion of the dislocation mainly determines the length of the dislocation in the γ' phase. When the model fractures at a strain of 12.3% at high temperature, numerous dislocations are still distributed within the γ phase, while the length of dislocations in the γ' phase is zero. As the temperature increases, the dislocation length difference between the two-phase at the same strain shows an overall increasing trend. It has been shown that Shockley dislocation and stair-rod dislocation mainly affect the plastic de-

formation of nickel-based single crystal superalloys, and other dislocations such as Frank, Perfect, and Hirth dislocations are almost zero inside the material[13,35] and the statistics of dislocation lengths in Fig. 6 exhibit the same results. According to Figs. 6(c) and 6(d), the length of Shockley dislocation in both phases is much larger than that of Stair-rod dislocation. Shockley dislocation are the main microscopic manifestation of plastic deformation in the model.

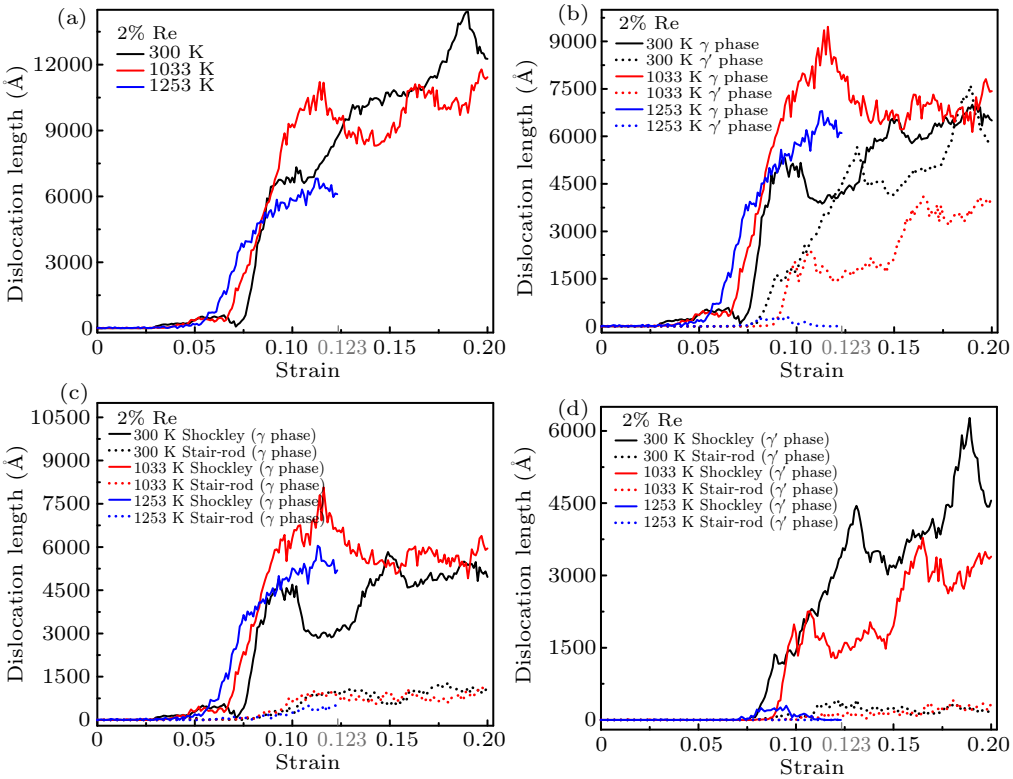


Fig. 6. Dislocation length at different temperatures (2% Re): (a) total dislocation length, (b) dislocation length in the γ and γ' phases, (c) length of Shockley dislocation and stair-rod dislocation in the γ phase, (d) length of Shockley dislocation and stair-rod dislocation in the γ' phase.

3.4. Plastic deformation mechanisms

3.4.1. Plastic deformation at a temperature of 300 K

As shown in Fig. 7(a), at 300 K and 7.6% strain, dislocations nucleate at the edge of the hole in the γ phase, initiating plastic deformation. Stacking faults are distributed along the {111} slip planes. There is no dislocation in the γ' phase, and it is still in the elastic deformation stage. At this point, the γ phase has a strain of 3.97%, the γ' phase has a strain of 3.63%, and the strain difference between the two phases is 0.34%. At 8.3% strain, as shown in Fig. 7(b), dislocations generated at the edge of the hole move along the {111} slip planes in the γ phase, increasing its strain to 4.42%. Meanwhile, some Shockley dislocations cut through the hole interface into the γ' phase, and the γ' phase begins to gradually undergo plastic deformation, and the strain is 3.88%. The strain difference between the two phases is 0.54%. At 10.4% strain, as shown in Fig. 7(c), dislocations continue to cut the hole interface into the γ' phase. A large number of dislocations move along the {111} slip planes in the γ phase. The dislocations will cut the periodic boundary into the γ' phase. At this point, the γ phase has a strain of 5.54%, the γ' phase has a strain of 4.86%, and the strain difference between the two phases is 0.68%. When the strain increases to 20%, the dislocation distribution in the two phases gradually tends to be balanced. At this point, the γ phase strain is 10.56%, and the γ' phase strain is 9.44%. The difference between the two phases is 1.12%.

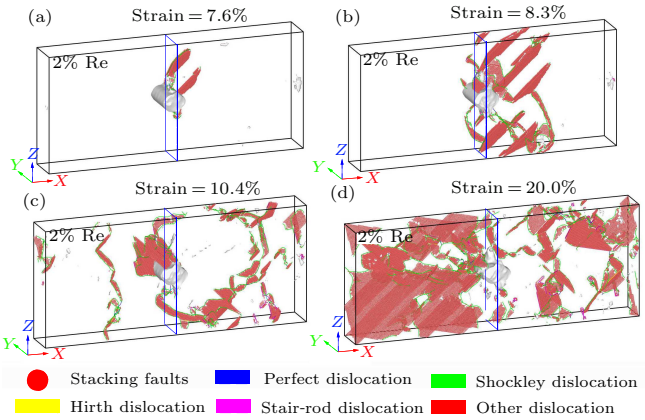


Fig. 7. Dislocation morphology in the γ–γ' phase at temperature 300 K (2% Re): (a) strain = 7.6%, (b) strain = 8.3%, (c) strain = 10.4%, (d) strain = 20.0%.

At all four strain nodes in Fig. 7 above, the strain of the γ phase is greater than that of the γ' phase. As the strain increases, the strain difference between the two-phase increases from 0.34% at the beginning of plastic deformation in the γ phase to 1.12% at the end of the deformation. In both the elastic and plastic deformation phases, the γ phase undergoes more deformation and has a larger dislocation length. This result

is also consistent with the data in Fig. 6, where the γ' phase has better elastic–plastic deformation resistance. At strains of 7.6%, 8.3%, 10.4%, and 20%, the strain of the γ' phase as a percentage of the total strain is 47.76%, 46.75%, 46.73%, and 47.2%, respectively. At the corresponding four deformation stages, the average strain rate of the γ phase is larger than that of the γ' phase. In the elastic deformation phase, the γ and γ' phases deform synchronously, both undergo elastic deformation, and the difference between the average strain rates of the two-phase is small. When the strain increases from 7.6% to 8.3%, the deformation of the two-phase is not synchronized. The γ phase undergoes plastic deformation, while the γ' phase undergoes elastic deformation, and the deformation is in an unstable state. When the strain increases from 8.3% to 10.4%, the γ' phase starts to undergo plastic deformation gradually. The dislocations in the γ phase expand rapidly, and the deformation difference between the two-phase is still large, and the average strain rate difference decreases. When the strain increases from 10.4% to 20%, stable plastic deformation occurs in the two-phase, and the average strain rate difference reaches the minimum value. The asynchronism of the two-phase plastic deformation is an important reason for the difference in deformation between the two-phase, causing the two-phase interface to be in an unstable state and becoming an important source of failure.

As shown in Fig. 8(a), at 8.8% strain, Shockley dislocations $1/6\ [12\bar{1}]$ and $1/6\ [211]$ move along the $(\bar{1}11)$ plane. When the strain is increased to 8.9%, as shown in Fig. 8(b), $1/6\ [12\bar{1}]$ and $1/6\ [211]$ Shockley dislocations bundle integrates with the perfect screw dislocation $1/2\ [110]$, the perfect screw dislocation cross-slip to the $(1\bar{1}1)$ plane, and decomposes into two Shockley dislocations with stacking faults in the middle.[36] The dislocation reaction is as follows:

$$\frac{1}{6}\left[12\bar{1}\right]+\frac{1}{6}\left[211\right]+SF_{(\bar{1}11)}\rightarrow\frac{1}{2}\left[110\right], \tag{1}$$

$$\frac{1}{2}\left[110\right]\rightarrow\frac{1}{6}\left[121\right]+\frac{1}{6}\left[21\bar{1}\right]+SF_{(1\bar{1}1)}. \tag{2}$$

With the movement and reaction of dislocations, as shown in Fig. 8(c), a strain of 9.0% produces a $1/3\ [00\bar{1}]$ Hirth edged dislocation at the intersection line between the plane and the plane. This dislocation cannot slip on the $\{111\}$ planes and plays a fixed role in the adjacent extended dislocation, which can hinder the movement of the dislocation and make the material have better plastic deformation resistance.

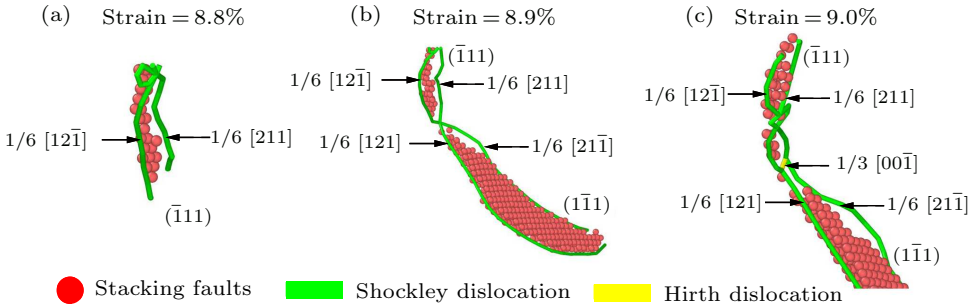


Fig. 8. Cross-slip of dislocation at temperature 300 K (2% Re): (a) strain = 8.8%, (b) strain = 8.9%, (c) strain = 9.0%.

In the early stage of plastic deformation, dislocations nucleate first and move in the γ phase at the edge of the hole, and only a small number of dislocations can cut into the γ' phase. Dislocations in the two-phase move along the $\{111\}$ slip planes. The γ' phase has a lower dislocation density than the γ phase and exhibits obstruction to dislocation movement, resulting in strong plastic deformation resistance. As the strain increases, the dislocations moving to the periodic boundary of the two phases begin to cut the periodic boundary into the γ' phase. The plastic deformation mode of the γ' phase changes and plastic deformation intensifies. More dislocations cut the two-phase interface into the γ' phase, and the plastic deformation resistance of the γ' phase is weakened. The movement of dislocations is mainly slip, cross-slip, and shearing into the γ' phase.

3.4.2. Plastic deformation at a temperature of 1033 K

As shown in Fig. 9(a), at 1033 K and 6.9% strain, dislocations nucleate at the edge of the hole in the γ phase, initiating plastic deformation. The γ phase has a strain of 4.05%, while the γ' phase has no dislocations and a strain of 2.85%. The strain difference between the two phases is 1.2%. When the strain reaches 9.2%, as shown in Fig. 9(b), dislocations move to the periodic boundary, and a few cut through the periodic boundary into the γ' phase. Dislocations are mainly distributed in the γ phase. At this point, the γ phase strain is 5.99%, and the γ' phase strain is 3.21%. The difference between the two phases is 2.78%. When the strain reaches 10.1%, as shown in Fig. 9(c), dislocations continue to cut through the hole interface into the γ' phase. Many dislocations move along the $\{111\}$ slip planes in the γ phase. At this point, the γ phase has a strain of 6.49%, the γ' phase has a strain of 3.61%, and the strain difference between the two phases is 2.88%. When the strain reaches 20%, the dislocation length difference in the two phases decreases, but the dislocations are mainly distributed in the γ phase. At this point, the γ phase has a strain of 11.52%, the γ' phase has a strain of 8.48%, and the strain difference between the two phases is 3.04%.

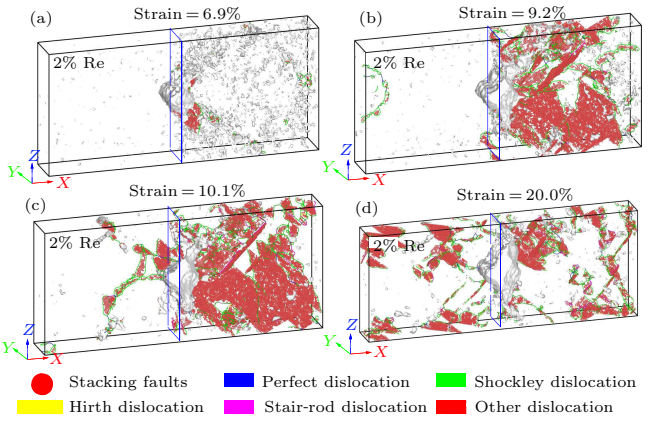


Fig. 9. Dislocation morphology in the γ–γ' phase at temperature 1033 K (2% Re): (a) strain = 6.9%, (b) strain = 9.2%, (c) strain = 10.1%, (d) strain = 20.0%.

In Fig. 9, at the four strain nodes, the γ phase has a larger strain than the γ' phase. The strain difference increases from 1.2% at the start of γ phase plastic deformation to 3.04% at the end, suggesting that the γ phase undergoes more elastic and plastic deformation at 1033 K. At strains of 6.9%, 9.2%, 10.1%, and 20%, the proportion of strain in the γ' phase to the total strain is 41.30%, 34.90%, 35.74%, and 42.40%, respectively. The average strain rate of the γ phase is larger than that of the γ' phase in the corresponding four deformation stages. The two-phase strain rate difference in the four phases has the same variation rule as that at 300 K. When the plastic deformation of the two phases is not synchronized, the strain rate difference reaches the maximum, while in the stable plastic deformation stage, the strain rate difference decreases to the minimum. Compared to 300 K, at 1033 K, the proportion of γ' phase strain to total strain decreases at the four strain nodes. This indicates a larger dislocation length difference between the two-phase at medium temperature, consistent with the statistical results in Fig. 6(b). As the temperature increases, thermal activation makes the movement of the dislocation more active, so that the γ phase undergoes more plastic deformation.

At a strain of 10.3%, a single dislocation appears at the top of the arc of the semicircular hole in the γ' phase and disappears after a strain increase of 0.1%, as shown in the blue circle in the enlarged view of Fig. 10. Unlike dislocations that cut through the interface into the γ' phase, this single dislocation generates in the γ' phase. Due to the nucleation at the edge of the hole, the dislocation is quickly annihilated after generation. Compared with 300 K, the plastic deformation of the γ' phase at 1033 K shows new characteristics. In addition, a single dislocation appears at the top of the arc of the semicircular hole at 16.7% strain and disappears at 16.8% strain.

As the temperature rises, the movement of atoms intensifies, and vacancies and point defects are easily generated in the material. These vacancies and point defects make the dislocation more likely to climb. When the strain is 15.4%, as shown in Fig. 11(a), a perfect dislocation with the Burgers vector of $1/2\ [\bar{1}\bar{1}0]$ is observed in the γ' phase. In the red circles and the red boxes of the microscopic magnification, we can see the dislocation jog formed by the dislocation climbing in the directions of $[1\bar{1}1]$ and $[1\bar{1}\bar{1}]$ respectively. When the strain increases to 15.6%, as shown in Fig. 11(b), the morphology of the $1/2\ [\bar{1}\bar{1}0]$ perfect dislocation changes with the climbing motion, forming more dislocation jog, as shown in the red circles and red boxes in the enlarged figure. This indicates that the dislocation underwent a more intense climbing motion as the strain increased. Different from 300 K, the plastic deformation at 1033 K is mainly manifested as the slip of dislocations, the shearing into γ' phase and the climbing of dislocations.

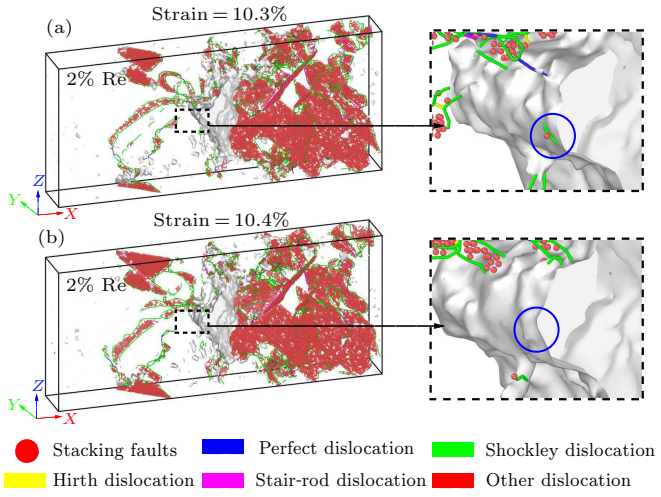


Fig. 10. Dislocations at the top of the arc of the γ' phase semicircular hole at temperature 1033 K (2% Re): (a) strain = 10.3%, (b) strain = 10.4%.

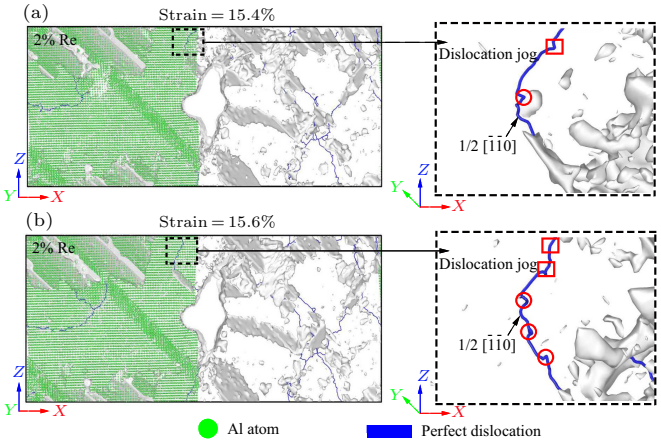


Fig. 11. Climbing process of dislocations at temperature 1033 K (2% Re): (a) strain = 15.4%, (b) strain = 15.6%.

3.4.3. Plastic deformation at a temperature of 1253 K

At 1253 K and a strain of 6.5%, as shown in Fig. 12(a), dislocations nucleate at the edge of the hole in the γ phase, initiating plastic deformation. At this point, the γ phase has a strain of 3.84%, while no dislocations appear in the γ' phase, which has a strain of 2.66%. The strain difference between the two phases is 1.18%. When the strain reaches 7.9%, as shown in Fig. 12(b), dislocations move along the {111} slip

planes in the γ phase, producing numerous stacking faults. A few dislocations cut through the periodic boundary into the γ' phase. At this point, the γ phase has a strain of 4.87%, the γ' phase has a strain of 3.03%, and the strain difference between the two phases is 1.84%. When the strain is 12.3%, the model fractures and there are still a large number of dislocations and stacking faults in the γ phase, and the strain of the γ phase is 11.18%. From the beginning of tensile loading until the material fractures, no dislocations cut through the hole interface into γ' phase. The dislocations that cut through the periodic boundary and enter the γ' phase annihilate at the hole. Therefore, there is no dislocation in the γ' phase at the time of fracture. The strain in the γ' phase is 1.12%, while the strain difference between the two phases is 10.06%. It is worth noting that when the strain reaches the critical point of 10.4%, the semi-circular hole in the γ phase is severely deformed. This again proves that 10.5% is a critical strain point beyond which the two-phase model enters a rapid fracture stage. To maintain the stability of the model strain, the strain of the γ' phase begins to decrease with the increase of the total strain. At this time, the strain of the γ phase and the γ' phase are 7.41% and 2.99%, respectively, and the strain difference between the two phases is 4.42%.

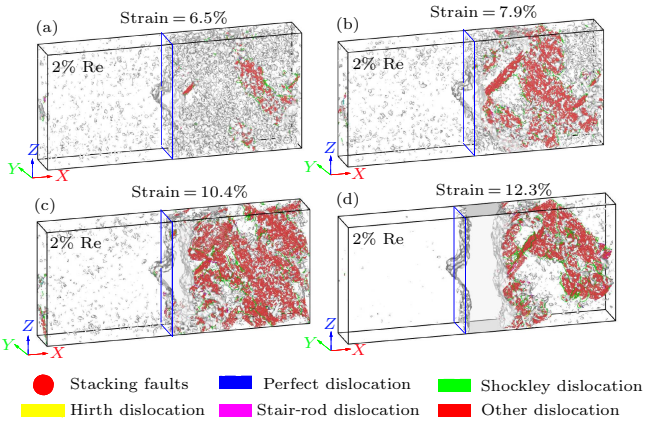


Fig. 12. Dislocation morphology in the γ–γ' phase at temperature 1253 K (2% Re): (a) strain = 6.5%, (b) strain = 7.9%, (c) strain = 10.4%, (d) strain = 12.3%.

At the four strain nodes in Fig. 12 above, when the strain increases from 6.5% to 10.4%, the two corresponding variations increase from 1.18% to 4.42%, and the proportion of the γ' phase strain in the total strain is 40.92%, 38.35%, and 28.75%, respectively. In the corresponding three deformation stages, the average strain rate of γ phase is higher than that of γ' phase. The γ phase also undergoes more elastic–plastic deformation at 1253 K, as at low and medium temperatures. Different from the medium and low temperatures, the deformation of the model is more intense at high temperature. The difference in the average strain rate of the two-phase in the three stages increases continuously. This phenomenon also corresponds to the stress–strain curve in Fig. 4, where a stable plastic deformation phase is lacking at high temperatures.

Similar to 1033 K, at 1253 K and 7.5% strain, a single dislocation appears at the arc top of the semi-circular hole in the γ' phase, which annihilates at 7.6% strain, as shown in the blue circle in the enlarged figure in Fig. 13. During the continuous increase of the strain to 12.3%, such transient single dislocations occur several times at the top of the arc of the semicircular hole in the γ' phase. This indicates that the increase in temperature can promote the nucleation of such single dislocations. At high temperature, hole defect spreads rapidly in the γ phase, resulting in severe deformation of the semi-circular hole in the γ phase. This further causes a larger plastic deformation of the semi-circular hole in the γ' phase and causes a single dislocation to briefly exist at the edge of the hole in the γ' phase. From 1033 K to 1253 K, the increase in temperature resulted in more individual dislocations at the edge of the semicircular hole in the γ' phase.

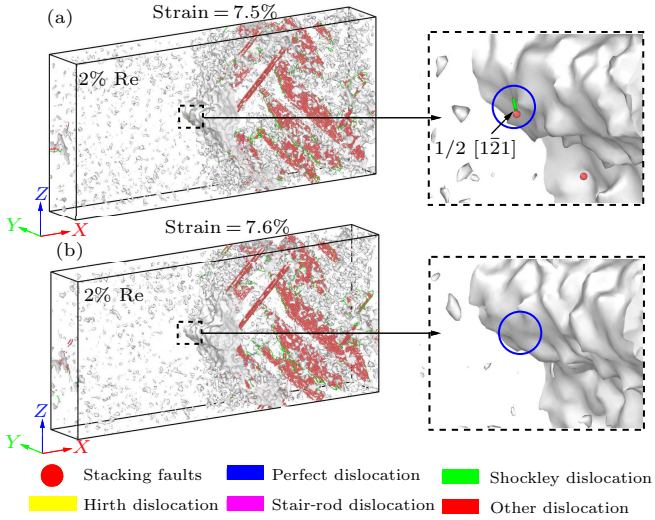


Fig. 13. Dislocations at the top of the arc of the γ' phase semicircular hole at temperature 1253 K (2% Re): (a) strain = 7.5%, (b) strain = 7.6%.

At a temperature of 1253 K, when the strain is 9.2%, a perfect dislocation with a Burgers vector of $1/2\ [10\bar{1}]$ is observed at the atomic gap within the γ' phase as shown in Fig. 14(a). This perfect dislocation climbs along the $[\bar{1}1\bar{1}]$ and $[\bar{1}\bar{1}\bar{1}]$ directions, resulting in the formation of dislocation jog, as shown within the red circles and red boxes of the enlarged figure. When the strain increases to 9.4%, as shown in Fig. 14(b), the $1/2\ [10\bar{1}]$ perfect dislocation continues to climb, producing more dislocation jog, as shown in the red circles and red boxes of the enlarged figure. The dislocation morphology changes due to the climbing motion as the strain increases from 9.2% to 9.4%. It has been shown that dislocations are more prone to climbing at high temperatures,[12] which is also consistent with the simulation results in this paper.

Due to the periodic boundary conditions used in the simulation, the model was doubled along the X-axis in order to more intuitively observe the interaction between the dislocation and the γ' phase, as shown in Fig. 15(a). When the strain

is 12.2%, a large number of dislocation loops can be observed within the γ phase and at the periodic boundary of the model, which are shown in Figs. 15(b) and 15(c), respectively. After the dislocations move and meet on the {111} slip planes, they interact with each other and entangle to form dislocation nodes. These nodes have a fixed effect on the dislocations, causing the dislocations between the nodes to bend and form a dislocation loop, as shown in Fig. 15(b). With increasing strain, dislocation loops proliferate within the γ phase[11] and this large distribution of dislocations within the matrix phase can promote rafting in the γ' phase.[37] As the temperature increases, the stacking fault energy increases. It is difficult to cut the γ' phase when the dislocation slips to the periodic interface,[12,25] and the impeded dislocation bends at the two-phase interface, thus forming a dislocation loop, as shown in Fig. 15(c). The γ' phase exhibits obvious Orowan enhancement, and the dislocation loops formed by Orowan bending of the dislocations at the interface of the two-phase after being hindered are also observed in the experiments[12] and molecular dynamics simulations.[16,22] Unlike at low and medium temperatures, the plastic deformation of the two-phase at 1253 K is mainly characterized by the slip of dislocations, shearing of the γ' phase, dislocation climbing, and the Orowan mechanism.

The plastic deformation mechanism of the two-phase changes significantly with the increase in temperature. At low, medium, and high temperatures, the dislocations nucleate first at the edge of the hole in the γ phase and then slip into the γ phase with a large number of stacking faults. With the increase of strain, the dislocation continuously cuts the two-phase interface into the γ' phase, and the dislocation movement is accompanied by the phenomenon of cross-slip. At the medium and high temperatures, the dislocation also began to climb, and a single dislocation existed briefly at the top of the arc of the semicircular hole in the γ' phase. At high temperature, the dislocations bend Orowan and form dislocation loops. Temperature affects the shear of the dislocation to the γ' phase. At medium and low temperatures, the dislocation can cut the hole interface and the periodic boundary into the γ' phase. At high temperature, with the increase of strain, the semi-circular hole in the γ phase deforms rapidly and violently, and the deformation affects almost the entire longitudinal section along the Y–Z axes. Before deformation, a gradient stress concentration area is formed in the γ phase. The higher stress concentration causes the dislocation to expand in the γ phase, making it difficult for the dislocation to cut the hole interface into the γ' phase. The rapid and violent deformation of the hole along the longitudinal section also prevents the dislocation from cutting the hole interface. Therefore, the dislocation only cuts through the periodic boundary into the γ' phase at high temperature. At low, medium and high temperatures, the γ phase has a larger average strain rate and carries the main deformation in different deformation stages. The difference in average strain rate between the two-phase increases due to the non-synchronous plastic deformation.

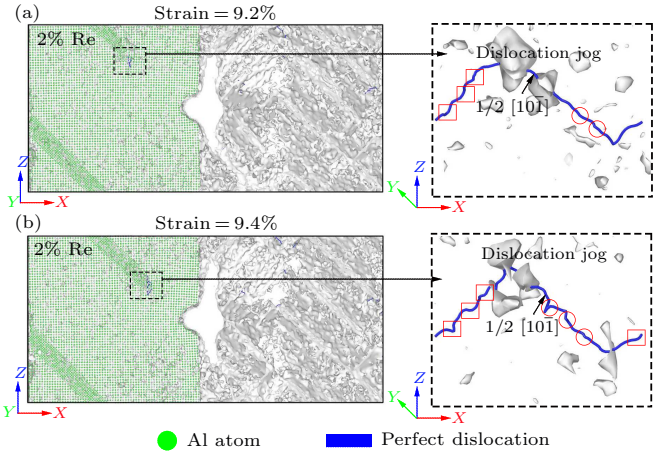


Fig. 14. Climbing process of dislocations at temperature 1253 K (2% Re): (a) strain = 9.2%, (b) strain = 9.4%.

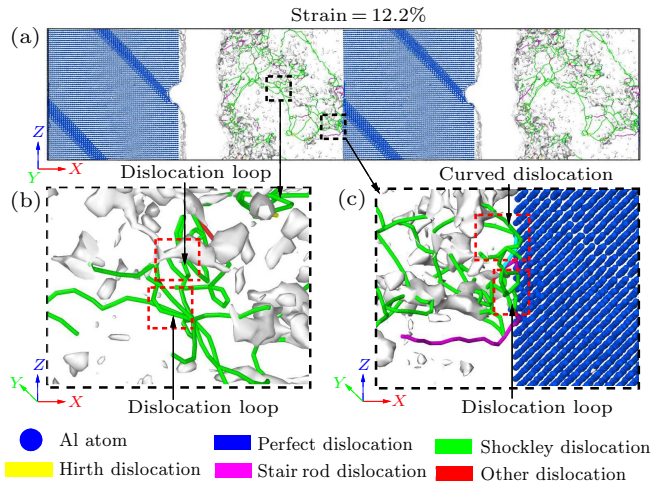


Fig. 15. Dislocation loops at temperature 1253 K (2% Re): (a) Dislocation distribution at 12.2% strain, (b) dislocation loops within the γ phase, (c) dislocation loops at the periodic boundary of the two-phase.

4. Conclusion

In this paper, the elastic–plastic behavior of the γ–γ' phase of nickel-based single crystal superalloys has been investigated using molecular dynamics methods, and the main conclusions are as follows.

(i) The addition of Re makes the dislocation mainly distributed in the γ phase. The higher the Re content, the earlier the γ phase yields, while the γ' phase yields later. When the Re content is between 0% and 2%, the inhibitory effect of Re on dislocations increases as the Re content increases. However, when the Re content is between 2% and 5%, the inhibitory effect of Re on dislocation decreases as the Re content increases.

(ii) Dislocations nucleate first in the γ phase, resulting in plastic deformation of the γ phase before the γ' phase. As the strain increases, the length of dislocations is unchanged at first, then grows rapidly, and finally fluctuates and changes. The length of dislocations in the γ phase is larger than that of

the γ' phase at different temperatures. The length of dislocations decreases with the increase in temperature.

(iii) Temperature can affect the movement of dislocation. Superalloys have different plastic deformation mechanisms at low temperature, medium temperature, and high temperature. The way dislocations cut the γ' phase varies with temperature. At low and medium temperatures, dislocations cut the hole interface and the periodic boundary into the γ' phase. At high temperature, dislocations cut the periodic boundary into the γ' phase.

Acknowledgement

Project supported by the Xi'an Science and Technology Plan Project of Shaanxi Province of China (Grant No. 23GXFW0086).

References

[1] Liu L P, Cao J, Guo W and Wang C Y 2022 *Chin. Phys. B* **31** 016105
[2] Liu C P, Zhang X N, Ge L, Liu S H, Wang C Y, Yu T, Zhang Y F and Zhang Z 2017 *Mater. Sci. Eng. A* **682** 90
[3] Wen Z X, Liang J W, Liu C Y, Pei H Q, Wen S F and Yue Z F 2018 *Int. J. Mech. Sci.* **141** 276
[4] Xiong X H, Quan D M, Dai P D, Wang Z P, Zhang Q X and Yue Z F 2015 *Mater. Sci. Eng. A* **636** 608
[5] Caccuri V, Cormier J and Desmorat R 2017 *Mater. Des.* **131** 487
[6] Wollgramm P, Buck H, Neuking K, Parsa A B, Schuwalow S, Rogal J, Drautz R and Eggeler G 2015 *Mater. Sci. Eng. A* **628** 382
[7] Wu R H, Zaiser M and Sandfeld S 2017 *Int. J. Plast* **95** 142
[8] Liu J L, Yu J J, Jin T, Sun X F, Guan H R and Hu Z Q 2011 *Trans. Nonferrous Met. Soc. China* **21** 1518
[9] Shi Z X, Liu S Z, Yu J and Li J R 2015 *J. Iron Steel Res. Int.* **22** 738
[10] Tan Z H, Wang X G, Du Y L, Duan T F, Yang Y H, Liu J L, Liu J D, Yang L, Li J G, Zhou Y Z and Sun X F 2020 *Mater. Sci. Eng. A* **776** 138997
[11] Wang G L, Liu J L, Liu J D, Wang X G, Zhou Y Z, Sun X D, Zhang H F and Jin T 2017 *Mater. Des.* **130** 131
[12] Lv P S, Liu L R, Zhao G Q, Guo S D, Zhou Z R, Zhao Y S and Zhang J 2022 *J. Alloys Compd.* **926** 166819
[13] Wu R H, Yin Q, Wang J P, Mao Q Z, Zhang X and Wen Z X 2021 *J. Alloys Compd.* **862** 158643
[14] Shang J, Yang F, Li C, Wei N and Tan X 2018 *Comput. Mater. Sci.* **148** 200
[15] Yin Q, Wu R H, Wang J P, Chen S Q, Lian Y D and Wen Z X 2021 *Mech. Mater.* **160** 103989
[16] Chen B, Wu W P, Chen M X and Guo Y F 2020 *Comput. Mater. Sci.* **185** 109954
[17] Ding Q Q, Li S Z, Chen L Q, Han X D, Zhang Z, Yu Q and Li J X 2018 *Acta Mater.* **154** 137
[18] Wu X X, Makineni S K, Liebscher C H, Dehm G, Mianroodi J R, Shanthraj P, Svendsen B, Buerger D, Eggeler G, Raabe D and Gault B 2020 *Nat. Commun.* **11** 1076
[19] Yao X, Ding Q Q, Wei X, Wang J, Zhang Z and Bei H B 2022 *J. Alloys Compd.* **926** 166835
[20] Zhang Z K and Yue Z F 2018 *J. Alloys Compd.* **746** 84
[21] Li P, Li Q Q, Jin T, Zhou Y Z, Li J G, Sun X F and Zhang Z F 2014 *Mater. Sci. Eng. A* **603** 84
[22] Wu W P, Ding Z J, Chen B, Shen H F and Li Y L 2022 *J. Mater. Res. Technol-JMRT* **18** 5144
[23] Liu L, Meng J, Liu J L, Zou M K, Zhang H F, Sun X D and Zhou Y Z 2019 *J. Mater. Sci. Technol.* **35** 1917
[24] Zhang J C, Huang T W, Lu F, Cao K L, Wang D, Zhang J, Zhang J, Su H J and Liu L 2021 *J. Alloys Compd.* **876** 160114
[25] Li P, Li Q Q, Jin T, Zhou Y Z, Li J G, Sun X F and Zhang Z F 2014 *Int. J. Fatigue* **63** 137
[26] Long H B, Liu Y N, Mao S C, Wei H, Zhang J X, Ma S Y, Deng Q S, Chen Y H, Zhang Z and Han X D 2018 *Intermetallics* **94** 55
[27] Rae C M F and Reed R C 2001 *Acta Mater.* **49** 4113
[28] Zhang Z K, Wen Z X and Yue Z F 2020 *Appl. A-Mater. Sci. Process.* **126** 680
[29] Plimpton S 1995 *J. Comput. Phys.* **117** 1
[30] Du J P, Wang C Y and Yu T 2013 *Model. Simul. Mater. Sci. Eng.* **21** 015007
[31] Pun G P P and Mishin Y 2009 *Philos. Mag.* **89** 3245
[32] Stukowski A 2010 *Model. Simul. Mater. Sci. Eng.* **18** 015012
[33] Stukowski A, Bulatov V V and Arsenlis A 2012 *Model. Simul. Mater. Sci. Eng.* **20** 085007
[34] Yue E L, Yu T, Wang Y J and Wang C Y 2021 *Intermetallics* **132** 107133
[35] Wang J P, Liang J W, Wen Z X and Yue Z F 2019 *Comput. Mater. Sci.* **160** 245
[36] Xiong T W, Chen X P, Lin Y P, He X F, Yang W, Hu W Y, Gao F and Deng H Q 2023 *Chin. Phys. B* **32** 020206
[37] Pettinari F, Douin J, Saada G, Caron P, Coujou A and Clément N 2002 *Mater. Sci. Eng. A* **325** 511